Angewandte Zuschriften

Lithium–Sulfur Batteries | Hot Paper

Deutsche Ausgabe: DOI: 10.1002/ange.201506972
Internationale Ausgabe: DOI: 10.1002/anie.201506972

Hollow Carbon Nanofibers Filled with MnO_2 Nanosheets as Efficient Sulfur Hosts for Lithium–Sulfur Batteries

*Zhen Li, Jintao Zhang, and Xiong Wen (David) Lou**

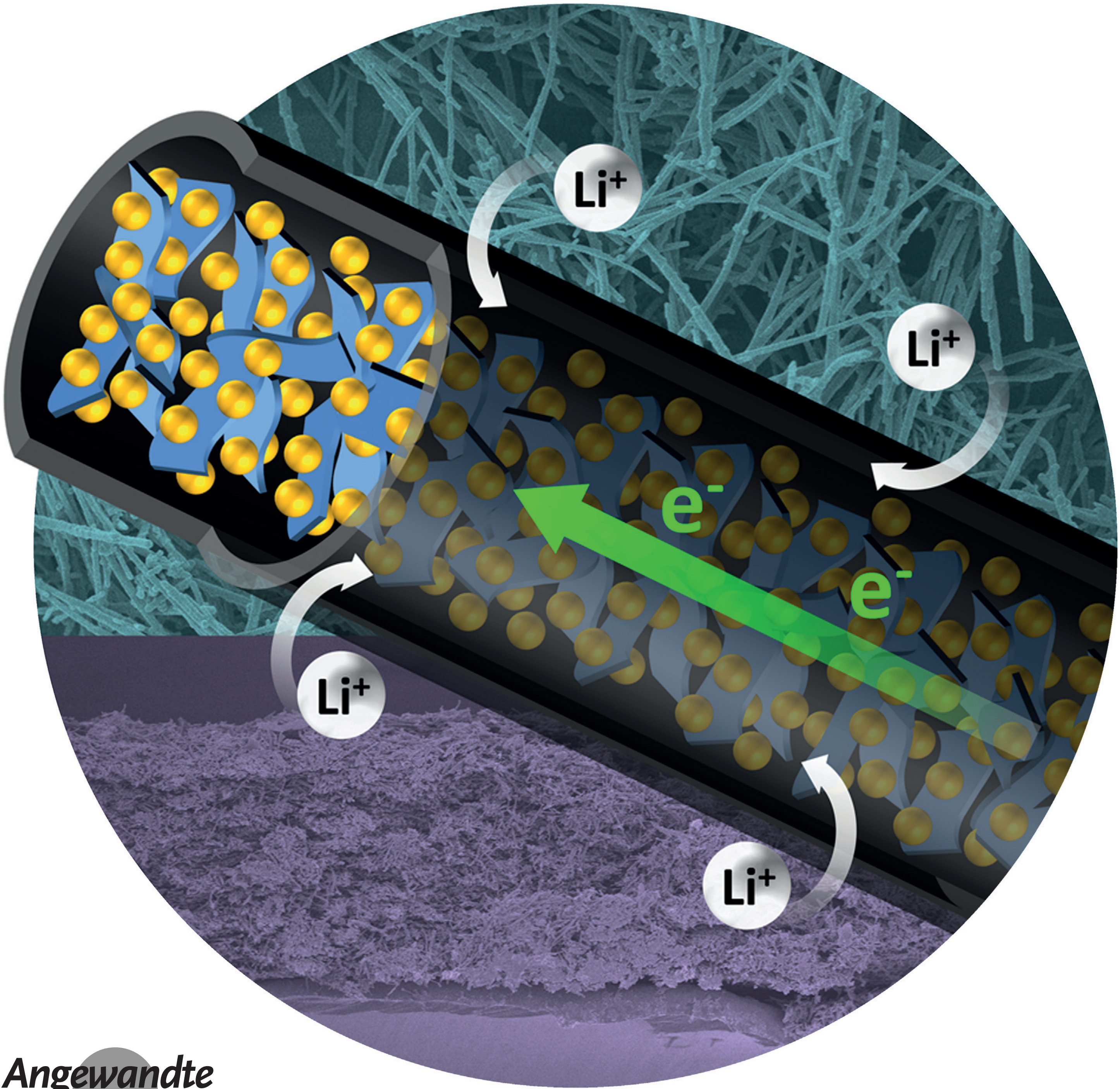

Abstract: *Lithium–sulfur batteries have been investigated as promising electrochemical-energy storage systems owing to their high theoretical energy density. Sulfur-based cathodes must not only be highly conductive to enhance the utilization of sulfur, but also effectively confine polysulfides to mitigate their dissolution. A new physical and chemical entrapment strategy is based on a highly efficient sulfur host, namely hollow carbon nanofibers (HCFs) filled with MnO_2 nanosheets. Benefiting from both the HCFs and birnessite-type MnO_2 nanosheets, the MnO_2@HCF hybrid host not only facilitates electron and ion transfer during the redox reactions, but also efficiently prevents polysulfide dissolution. With a high sulfur content of 71 wt% in the composite and an areal sulfur mass loading of 3.5 mg cm^{-2} in the electrode, the MnO_2@HCF/S electrode delivered a specific capacity of 1161 mAh g^{-1} (4.1 mAh cm^{-2}) at 0.05 C and maintained a stable cycling performance at 0.5 C over 300 cycles.*

Rechargeable batteries with sulfur-based cathodes have recently attracted great interest owing to various advantages, such as very high theoretical energy densities, extremely low costs, and nontoxicity.[1] Considering its multi-electron electrochemical redox reactions, sulfur has a theoretical capacity of 1675 mAh g^{-1}, which is much higher than that of almost all known solid cathode materials.[2] As a result, lithium–sulfur (Li-S) batteries have been considered as a promising candidate for next-generation electric-energy storage systems, and have great potential in many emerging applications, such as electric vehicles (EVs) and large-scale stationary electric energy storage.[1] However, Li-S batteries have suffered from some significant challenges, including low capacities, rapid capacity fading, and low Coulombic efficiencies, which are due to the so-called shuttle effect.[3] The low utilization of sulfur is mainly caused by the insulating nature of sulfur and lithium sulfides. However, the main problem arises from the dissolution of the reaction intermediates in the organic electrolyte. This not only causes capacity decay, but also leads to the shuttle effect: A large proportion of the capacity is consumed by redox reactions of polysulfides at both the cathode and anode surfaces.[4]

To address these challenges, many strategies have been developed to enhance the conductivity of sulfur and suppress the dissolution of polysulfides, such as using conductive hosts for sulfur,[5] inserting interlayers,[6] and exploiting new electrolytes/additives.[7,8] Carbon materials have been considered as excellent host materials for sulfur because their high conductivity renders the various redox processes of sulfur well accessible, and owing to their high specific surface areas, the redox intermediates can be effectively trapped.[9] In pioneering work by Nazar and co-workers, the sulfur species were simply encapsulated within highly ordered mesoporous carbon, which led to a reversible capacity of up to 1320 mAh g^{-1}.[10] Since then, various carbon materials have been applied in Li-S batteries, such as meso/microporous carbon,[11–13] graphene,[14,15] carbon nanotubes,[16,17] and hollow carbon nanofibers/nanospheres.[18–20] Although these carbon–sulfur nanocomposites were shown to have a significantly enhanced specific capacity at the beginning, the capacity often decayed rapidly in the subsequent cycles because the carbon hosts are nonpolar and therefore less efficient in entrapping polar polysulfides.

Polar materials are thought to form relatively strong chemical bonds with lithium polysulfides, thus effectively keeping them within the cathode.[21,22] Inspired by this idea, many polar host materials for sulfur have been developed, which were based on TiO_2,[23] Ti_4O_7,[24,25] MnO_2,[26] and metal–organic frameworks (MOFs), for example.[27] As expected, the cycling stabilities of Li-S batteries based on these sulfur host materials were significantly better. However, these materials have a much lower conductivity than carbon materials, which inevitably compromises the rate capability and even the specific capacity. Therefore, it is still a great challenge to effectively restrict the electrochemical redox reactions of Li_2S_x species in the cathode and at the same time achieve high sulfur utilization even at high current densities. One possibility to satisfy these two requirements simultaneously is the use of hybrid structures of polar metal oxides and highly conductive carbon materials.

Herein, we report the rational design and fabrication of a one-dimensional (1D) composite nanoarchitecture, namely hollow carbon nanofibers filled with MnO_2 nanosheets (MnO_2@HCF) as the host for sulfur. This MnO_2@HCF composite has several apparent advantages. First, with an ultrahigh aspect ratio, these 1D nanofibers can easily form a 3D interconnected conductive network, which greatly reduces the resistance of electron and ion transport during the charge–discharge processes, thus giving rise to high rate capabilities. Furthermore, MnO_2 nanosheets in the monoclinic birnessite phase are an efficient sulfur host,[26] which can keep the polysulfides inside the hollow carbon fibers and promote stable redox activity over the whole lifetime of the cathode material. Moreover, each hollow carbon nanofiber serves as a nanoscale electrochemical reaction chamber, providing some degree of physical entrapment for the polysulfides. Remarkably, the MnO_2@HCF/S composite with 71 wt% sulfur and an areal sulfur loading as high as 3.5 mg cm^{-2} showed significantly enhanced cycling stability and an excellent rate capability.

The synthesis of the MnO_2@HCF hybrid structures is illustrated in Figure 1a (for experimental details, see the Supporting Information). First, MnO_2 nanowires were used as a hard template. After coating with SiO_2 and resorcinol formaldehyde (RF) resin, the composite was carbonized in N_2 atmosphere at 700 °C for three hours. The MnO_2@HCF structure was then obtained by removing the SiO_2 interlayer in NaOH aqueous solution. Sulfur was introduced into the MnO_2@HCF host by the melt-diffusion method. Benefiting from the efficient surface bonding between the MnO_2 nano-

[*] Dr. Z. Li, J. T. Zhang, Prof. X. W. Lou
School of Chemical and Biomedical Engineering
Nanyang Technological University
62 Nanyang Drive, Singapore 637459 (Singapore)
E-mail: xwlou@ntu.edu.sg
davidlou88@gmail.com
Homepage: http://www.ntu.edu.sg/home/xwlou/

Supporting information for this article is available on the WWW under http://dx.doi.org/10.1002/anie.201506972.

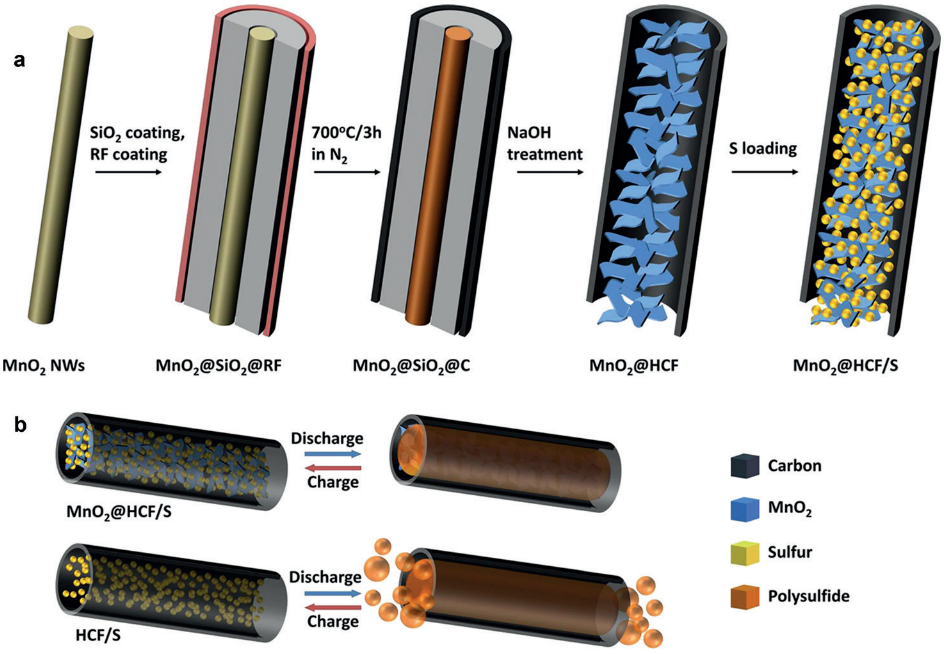

Figure 1. a) Synthesis of the MnO$_2$@HCF/S composite. b) Advantages of the MnO$_2$@HCF/S composite over HCF/S.

sheets and the sulfur species, the dissolution of polysulfides into the organic electrolyte was effectively mitigated during charge–discharge cycling (Figure 1 b).

Uniform MnO$_2$ nanowires with an average diameter of approximately 35 nm were prepared by a hydrothermal method (Supporting Information, Figure S1 a–c).[28] After coating with silica, the average diameter of the MnO$_2$@SiO$_2$ nanowires had increased to about 180 nm (Figure S1 d–f). The relatively thick SiO$_2$ layer serves as a spacer to generate sufficient internal void space in HCFs for accommodating a high sulfur content. Then, a thin RF layer was grown on the MnO$_2$@SiO$_2$ nanowires as the carbon precursor. After carbonization, the MnO$_2$@SiO$_2$@C coaxial nanowires well maintained the 1D morphology with an average diameter of approximately 290 nm. The thickness of the carbon sheath was estimated to be about 50 nm (Figure 2 a, d). Moreover, the carbon shell contained a large number of micropores (Figure S2), which is beneficial for the efficient transport of Li$^+$ ions. After treatment in NaOH aqueous solution, the SiO$_2$ layer had been completely etched while the carbon shells were left intact (Figure 2 b). Energy-dispersive X-ray (EDX) spectroscopy of the as-prepared MnO$_2$@HCF nanowires further confirmed the absence of SiO$_2$ (Figure S3). Interestingly, it was observed that the internal MnO$_2$ nanowires had been transformed into two-dimensional (2D) nanosheets after the NaOH treatment (Figure 2 e). This transformation apparently increases the surface area of MnO$_2$. Nitrogen sorption measurements of MnO$_2$@HCF revealed a high specific surface area of approximately 460 m^2 g^{-1} and a hierarchical mesoporous texture (Figure S4). As a result, the obtained MnO$_2$@HCF composite provides a much larger contact area for the mitigation of polysulfide dissolution owing to the strong interactions between MnO$_2$ and the polysulfides.[26] Sulfur was infiltrated into MnO$_2$@HCF by the melt-diffusion method. As shown in Figure 2 c, there is no deposition of sulfur particles on the outer surface of the MnO$_2$@HCF nanofibers, suggesting the complete diffusion of sulfur into the void space of the MnO$_2$@HCF composite. As sulfur is heavier than carbon, the dark region inside the carbon shell indicates the location of sulfur. This finding revealed that sulfur was homogeneously encapsulated within the hollow carbon fibers (Figure 2 f).

X-ray diffraction (XRD) analysis revealed the crystal phase changes of MnO$_2$ in each step. After sintering at 700 °C with carbon, α-MnO$_2$ was transformed into an amorphous phase (Figure S5) and then into monoclinic birnessite-type MnO$_2$ (JCPDS No. 43-1456) after the NaOH treatment (Figure 3 a).[29] This is consistent with a previous report that birnessite MnO$_2$ can be easily generated by heating manganese salts/oxides in alkaline solution at elevated temperature.[30] Thermogravimetric analysis (TGA) revealed that the MnO$_2$ content in the MnO$_2$@HCF composite was approximately 24 wt %, including about 7 wt % of water contained in the birnessite phase (Figure 3 b), which was mostly removed

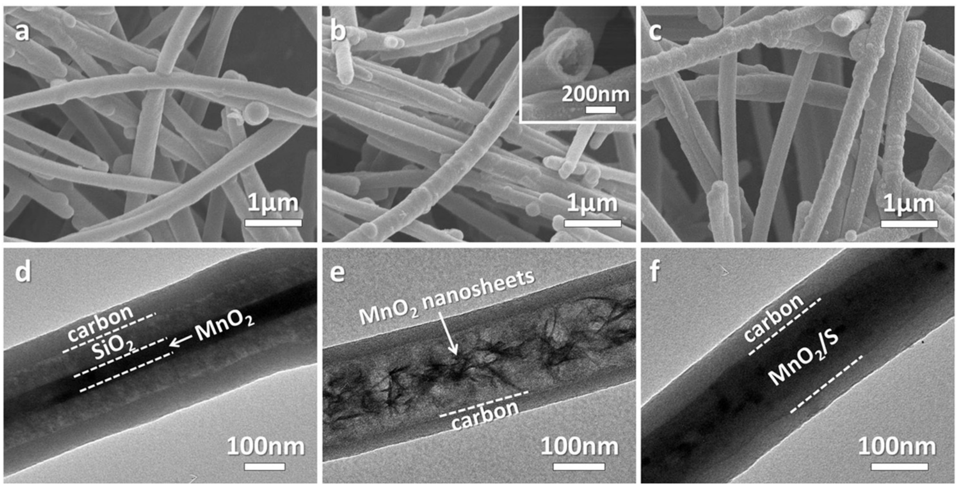

Figure 2. Field-emission scanning electron microscopy (FESEM) and transmission electron microscopy (TEM) images of a, d) MnO$_2$@SiO$_2$@C, b, e) MnO$_2$@HCF, and c,f) MnO$_2$@HCF/S.

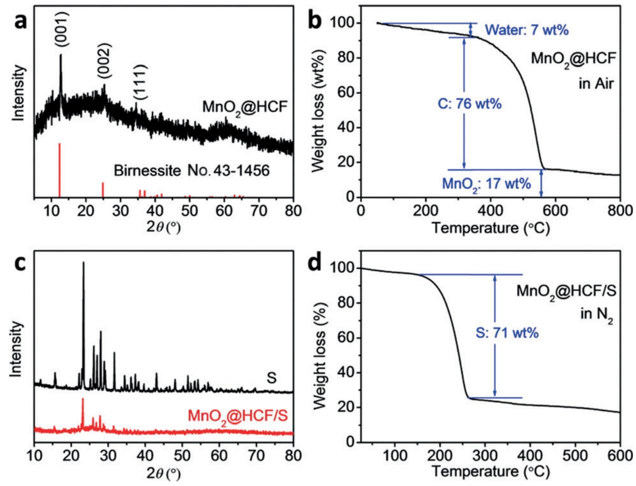

Figure 3. XRD patterns of a) MnO_2@HCF and c) MnO_2@HCF/S and pure sulfur. TGA curves of b) MnO_2@HCF in air and d) MnO_2@HCF/S in N_2 atmosphere with a heating rate of 10 °C min^{-1}.

during the subsequent sulfur loading process (Figure S6).[26,31] Birnessite-type MnO_2 nanosheets have been shown to be highly efficient polysulfide mediators,[26] which could not only prevent the dissolution of long-chain Li_2S_x ($x = 4$–8) into the organic electrolyte but also facilitate the deposition of solid-state Li_2S_x ($x = 1$–2). The XRD pattern of the MnO_2@HCF/S composite confirmed the presence of sulfur with the same orthorhombic structure as elemental sulfur powder (Figure 3c). The sulfur loading in the MnO_2@HCF/S composite was determined by TGA to be approximately 71 wt% (Figure 3d).

We next evaluated the electrochemical performance of the MnO_2@HCF/S nanocomposite as a cathode material for Li-S batteries. To meet the requirement of a high energy density, in our work, the areal sulfur loading was kept at approximately 3.5 mg cm^{-2}. To demonstrate the structural advantages of the MnO_2@HCF/S composite, a similar HCF/S nanocomposite was also prepared by removing the MnO_2 in MnO_2@HCF and evaluated for comparison. As shown in Figure 4a and b, the MnO_2@HCF/S composite delivered an initial discharge capacity of 1147 mAh g^{-1}, and more importantly, it was able to maintain a stable cycling performance for 100 charge–discharge cycles at 0.2 C. The rapid capacity decay in the first few cycles may be caused by the volumetric expansion and re-distribution of the active sulfur during the initial lithiation process. It was also confirmed that the MnO_2@HCF host contributed almost nothing to the measured capacity (Figure S7). For comparison, although the HCF/S nanocomposite delivered a slightly higher discharge capacity of 1216 mAh g^{-1} in the first cycle, it suffered from rapid capacity decay even in the first 40 cycles (Figure 4a and Figure S8). Moreover, the MnO_2@HCF/S electrode had a much high Coulombic efficiency than HCF/S, indicating that polysulfide dissolution into the organic electrolyte was effectively mitigated in the former, which was further confirmed through visual observation (Figure S9).

The rate capability of MnO_2@HCF/S was also evaluated by cycling at various current densities from 0.05 to 1 C (Figure 4c). At 0.05 C, the discharge capacity stabilized quickly at 1161 mAh g^{-1} (corresponding to an areal capacity of 4.1 mAh cm^{-2}). Further cycling capacities of 1090 (3.8), 1010 (3.5), 890 (3.1), and 690 mAh g^{-1} (2.4 mAh cm^{-2}) were measured at 0.1, 0.2, 0.5, and 1 C, respectively, confirming the excellent electronic/ionic transport properties and improved reaction kinetics (Figure 4d). When the current density was abruptly switched back to 0.05 C, most of the original capacity was recovered, indicating the excellent stability and reliability of the MnO_2@HCF/S composite structure. It should be pointed out that although the specific capacities at various current densities do not seem to be superior to those reported in other works, our material displayed a much higher areal capacity than slurry-coated electrodes (Figure S10). The high capacity of the electrode with such a high mass loading at various rate capabilities probably benefits from the 3D interconnected conductive network formed in the electrode (Figure S11). It is also important to point out that the introduction of MnO_2 does not significantly increase the impedance as confirmed by the similar impedance of the

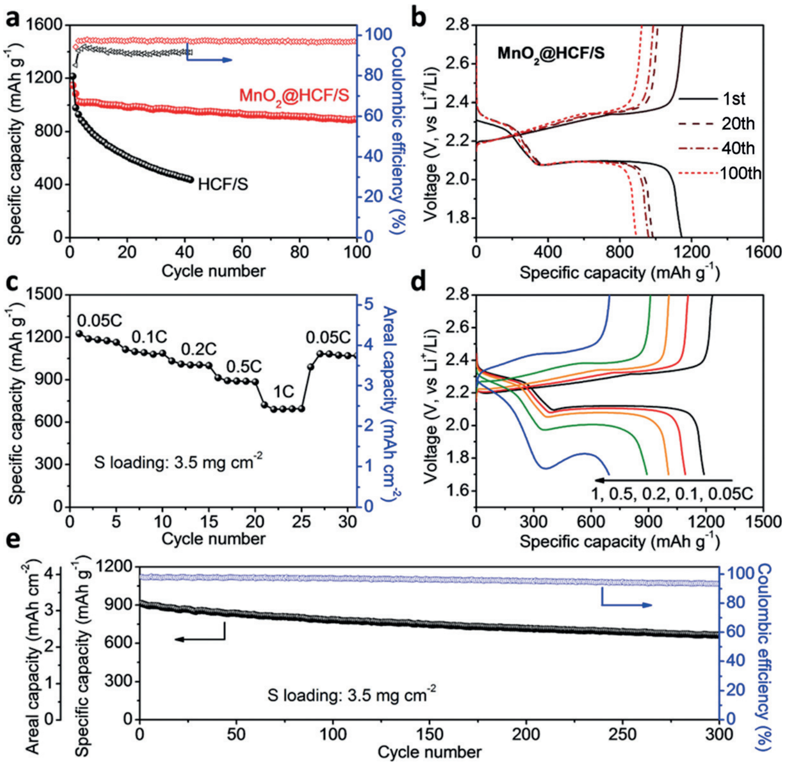

Figure 4. a) Cycle capacity and Coulombic efficiency of MnO_2@HCF/S in comparison with HCF/S at a current density of 0.2 C. b) Voltage profiles during cycling at 0.1 C. c) Discharge capacities. d) Voltage profiles at various rate capabilities from 0.05 to 1 C. e) Prolonged cycling performance of MnO_2@HCF/S at 0.5 C and the corresponding Coulombic efficiency. Areal capacity values were calculated based on the specific capacity and areal mass loading of sulfur.

MnO_2@HCF/S and HCF/S electrodes (Figure S12). The cycling stability was also studied at 0.5 C for 300 cycles (Figure 4e), over which the capacity gradually decreased to 662 mAh g^{-1} (2.3 mAh cm^{-2}). Considering the relatively high sulfur loading of 3.5 mg cm^{-2}, we consider this cycling performance to be excellent.

In summary, we have designed an integrated structure of hollow carbon nanofibers filled with MnO_2 nanosheets as a highly efficient host for the sulfur cathode. This structure benefits from both the physical entrapment of the polysulfides by the carbon shell and their chemical binding to the MnO_2 nanosheets. The nanofibers can easily form a 3D conductive network in the electrode, which facilitates electron and ion transfer during the charge–discharge process. Meanwhile, the MnO_2 nanosheets inside the hollow carbon nanofibers can chemically bind polysulfides and efficiently prevent their dissolution during the charge–discharge process. With this advanced design, a high sulfur loading of 71 wt% was achieved in the MnO_2/carbon/sulfur nanocomposite electrode. Remarkably, the obtained nanocomposite sulfur cathode with a very high areal sulfur density of 3.5 mg cm^{-2} delivered high specific capacities at different rate capabilities and an excellent cycling stability for 300 cycles. The present results show that with properly designed sulfur cathodes, lithium–sulfur batteries with high energy densities and improved cycle lifetimes might be eventually be developed.

Acknowledgements

X.W.L. is grateful to the Ministry of Education (Singapore) for financial support through the AcRF Tier 1 funding programme (RG12/14 and M4011258).

Keywords: electrochemistry · carbon nanofibers · lithium–sulfur batteries · manganese dioxide · nanosheets

How to cite: *Angew. Chem. Int. Ed.* **2015**, *54*, 12886–12890
Angew. Chem. **2015**, *127*, 13078–13082

[1] P. G. Bruce, S. A. Freunberger, L. J. Hardwick, J. M. Tarascon, *Nat. Mater.* **2012**, *11*, 19–29.
[2] X. L. Ji, L. F. Nazar, *J. Mater. Chem.* **2010**, *20*, 9821–9826.
[3] Y. X. Yin, S. Xin, Y. G. Guo, L. J. Wan, *Angew. Chem. Int. Ed.* **2013**, *52*, 13186–13200; *Angew. Chem.* **2013**, *125*, 13426–13441.
[4] Y. V. Mikhaylik, J. R. Akridge, *J. Electrochem. Soc.* **2004**, *151*, A1969.
[5] Y. Yang, G. Zheng, Y. Cui, *Chem. Soc. Rev.* **2013**, *42*, 3018–3032.
[6] Y. S. Su, A. Manthiram, *Nat. Commun.* **2012**, *3*, 1166.
[7] Z. Lin, Z. Liu, W. Fu, N. J. Dudney, C. Liang, *Angew. Chem. Int. Ed.* **2013**, *52*, 7460–7463; *Angew. Chem.* **2013**, *125*, 7608–7611.
[8] X. Liang, Z. Y. Wen, Y. Liu, M. F. Wu, J. Jin, H. Zhang, X. W. Wu, *J. Power Sources* **2011**, *196*, 9839–9843.
[9] Z. Li, Y. Huang, L. Yuan, Z. Hao, Y. Huang, *Carbon* **2015**, *92*, 41–63.
[10] X. L. Ji, K. T. Lee, L. F. Nazar, *Nat. Mater.* **2009**, *8*, 500–506.
[11] H. B. Wu, S. Wei, L. Zhang, R. Xu, H. H. Hng, X. W. Lou, *Chem. Eur. J.* **2013**, *19*, 10804–10808.
[12] Z. Li, Y. Jiang, L. Yuan, Z. Yi, C. Wu, Y. Liu, P. Strasser, Y. Huang, *ACS Nano* **2014**, *8*, 9295–9303.
[13] Z. Li, L. X. Yuan, Z. Q. Yi, Y. M. Sun, Y. Liu, Y. Jiang, Y. Shen, Y. Xin, Z. L. Zhang, Y. H. Huang, *Adv. Energy Mater.* **2014**, *4*, 1301473.
[14] Z. Wang, Y. Dong, H. Li, Z. Zhao, H. Bin Wu, C. Hao, S. Liu, J. Qiu, X. W. Lou, *Nat. Commun.* **2014**, *5*, 5002.
[15] M. Q. Zhao, Q. Zhang, J. Q. Huang, G. L. Tian, J. Q. Nie, H. J. Peng, F. Wei, *Nat. Commun.* **2014**, *5*, 3410.
[16] Z. Yuan, H. J. Peng, J. Q. Huang, X. Y. Liu, D. W. Wang, X. B. Cheng, Q. Zhang, *Adv. Funct. Mater.* **2014**, *24*, 6105–6112.
[17] Y. Fu, Y. S. Su, A. Manthiram, *Angew. Chem. Int. Ed.* **2013**, *52*, 6930–6935; *Angew. Chem.* **2013**, *125*, 7068–7073.
[18] C. Zhang, H. B. Wu, C. Yuan, Z. Guo, X. W. Lou, *Angew. Chem. Int. Ed.* **2012**, *51*, 9592–9595; *Angew. Chem.* **2012**, *124*, 9730–9733.
[19] N. Jayaprakash, J. Shen, S. S. Moganty, A. Corona, L. A. Archer, *Angew. Chem. Int. Ed.* **2011**, *50*, 5904–5908; *Angew. Chem.* **2011**, *123*, 6026–6030.
[20] G. Zheng, Q. Zhang, J. J. Cha, Y. Yang, W. Li, Z. W. Seh, Y. Cui, *Nano Lett.* **2013**, *13*, 1265–1270.
[21] C. J. Hart, M. Cuisinier, X. Liang, D. Kundu, A. Garsuch, L. F. Nazar, *Chem. Commun.* **2015**, *51*, 2308–2311.
[22] Q. Zhang, Y. Wang, Z. W. Seh, Z. Fu, R. Zhang, Y. Cui, *Nano Lett.* **2015**, *15*, 3780–3786.
[23] Z. Liang, G. Zheng, W. Li, Z. W. Seh, H. Yao, K. Yan, D. Kong, Y. Cui, *ACS Nano* **2014**, *8*, 5249–5256.
[24] X. Tao, J. Wang, Z. Ying, Q. Cai, G. Zheng, Y. Gan, H. Huang, Y. Xia, C. Liang, W. Zhang, Y. Cui, *Nano Lett.* **2014**, *14*, 5288–5294.
[25] Q. Pang, D. Kundu, M. Cuisinier, L. F. Nazar, *Nat. Commun.* **2014**, *5*, 4759.
[26] X. Liang, C. Hart, Q. Pang, A. Garsuch, T. Weiss, L. F. Nazar, *Nat. Commun.* **2015**, *6*, 5682.
[27] J. W. Zhou, R. Li, X. X. Fan, Y. F. Chen, R. D. Han, W. Li, J. Zheng, B. Wang, X. G. Li, *Energy Environ. Sci.* **2014**, *7*, 2715–2724.
[28] Y. Gao, Z. Wang, J. Wan, G. Zou, Y. Qian, *J. Cryst. Growth* **2005**, *279*, 415–419.
[29] C. H. Chen, V. M. Crisostomo, W. N. Li, L. Xu, S. L. Suib, *J. Am. Chem. Soc.* **2008**, *130*, 14390–14391.
[30] J. Zhou, L. Yu, M. Sun, S. Yang, F. Ye, J. He, Z. Hao, *Ind. Eng. Chem. Res.* **2013**, *52*, 9586–9593.
[31] Z. Liu, K. Xu, H. Sun, S. Yin, *Small* **2015**, *11*, 2182–2191.

Received: July 28, 2015
Revised: August 15, 2015
Published online: September 9, 2015

